5 Multiple-Quantum Magic-Angle Spinning (MQMAS)

5.1 How it Works

In 1995 Frydman and Harwood [1] proved the feasibility of a 2D NMR experiment that makes use of invisible multiple-quantum transitions combined with MAS to remove the anisotropy of the quadrupole interaction. Symmetric $p/2 \leftrightarrow -p/2$ coherences with the quantum level $p\mathrm{Q}$ were selected; in that case [1] $p = 3$, since the powder resonances are devoid of first-order quadrupole effects only for symmetric transitions. $3\mathrm{Q}$ denotes triple-quantum coherences, whereas $-1\mathrm{Q}$ represents usual single-quantum coherences.

The phase development, $\varphi(t)$, of single- or multiple-quantum coherences under MAS conditions is

$$\frac{\varphi(t)}{2\pi\, t} = \Delta\nu\; p \;+\; \nu_{p/2,-p/2} - \nu_{\mathrm{L}} = \Delta\nu\; p \;+ \nu_{\mathrm{iso}}(p) + \nu(p,\alpha,\beta,\eta) = \frac{\nu_{\mathrm{Q}}^2}{6\,\nu_{\mathrm{L}}} p \left\{ \begin{array}{c} \frac{1}{5}\left[I(I+1) - \frac{3}{4}p^2\right]\left(1 + \frac{\eta^2}{3}\right) \\ -\left[I(I+1) - \frac{17}{36}p^2 - \frac{5}{18}\right] g_{\mathrm{MAS}}(\alpha,\beta,\eta) \end{array} \right\}. \tag{5.01}$$

See Eq. (1.76) and the following modifications for MQMAS in Section 1.4. The anisotropic contribution is described by the function $g_{\mathrm{MAS}}(\alpha,\beta,\eta)$; see Table 1.2. The contributions from the chemical shift and from the resonance offset are included in $\Delta\nu = \sigma_{\mathrm{iso}}\nu_{\mathrm{L}} - \nu_{\mathrm{offset}}$. Eq. (5.01) shows that by going from the multiple-quantum level $p\mathrm{Q}$ to the $-1\mathrm{Q}$ level of observation, the sign of the phase development can be inverted. The influence of the anisotropy of the second-order quadrupole interaction is averaged out, if the times t_1 (between the first two pulses) and t_2 (after the last pulse), which were spent on the quantum levels $p\mathrm{Q}$ and $-1\mathrm{Q}$, respectively, fulfill the condition

$$\frac{t_2}{t_1} = p\,\frac{I(I+1) - \frac{17}{36}p^2 - \frac{5}{18}}{I(I+1) - \frac{3}{4}} = R(I,p). \tag{5.02}$$

This relation describes the appearance of the isotropic echo, and thus gives the slope $R(I,p)$ of the anisotropic axis, A, in the two-dimensional spectrum, which is obtained after the 2D Fourier transform with respect to t_2 and t_1. The pathway can be selected for a positive value of $R(I,p)$, since the sign of R changes if the sign of p is changed. This gives the echo at time t_2. For a negative value of $R(I,p)$ we obtain the so-called "antiecho" at time $-t_2$. Some values for $R(I,p)$ are $R(I=3/2, p=\pm3) = \mp 7/9$, $R(I=5/2, p=\pm3) = \pm 19/12$ and $R(I=5/2, p=\pm5) = \mp 25/12$.

Several pulse sequences can be used [2, 3] in order to excite a multiple-quantum coherence and convert it to the observable single-quantum coherence after the evolution time. The *z*-filter pulse sequence, which is shown in Fig. 5.1, was introduced in 1996 [4, 5] and is still in use. The highest possible RF power is applied for the first and second pulse. The first pulse excites multiple-quantum coherences, and the second pulse converts them back to zero-quantum coherences. With regard to ν_{RF} the third pulse (π/2) is about one order of magnitude weaker and correspondingly longer, in order to excite the central transition only. It converts non-observable zero-quantum coherences and populations ($p = 0$) into observable single-quantum coherences ($p = -1$). Fig. 5.1 shows the symmetric triple-quantum ($0 \rightarrow \pm3 \rightarrow 0 \rightarrow -1$) and the symmetric quintuple-quantum pathways ($0 \rightarrow \pm5 \rightarrow 0 \rightarrow -1$) for spin-5/2 nuclei. Although only one sign of p yields an echo that can be observed (see Eq. (5.02)), one must acquire both $\pm p$ coherence transfer pathways when trying to produce 2D MQMAS spectra that are free from dispersive distortions [2, 3, 6]. The symmetric pathway yields equal signal contributions from the echo and anti-echo pathways.

This leads to a cosine amplitude modulation of the time domain signal and a purely absorptive 2D spectrum [2]. The solid lines in Fig. 5.1 are the echo pathways, whereas the dashed lines represent the anti-echo pathways. The split-t_1 method, which will be considered in Section 5.3, also generates pure phase spectra, if the whole shifted echo is observed in the phase-modulated experiment.

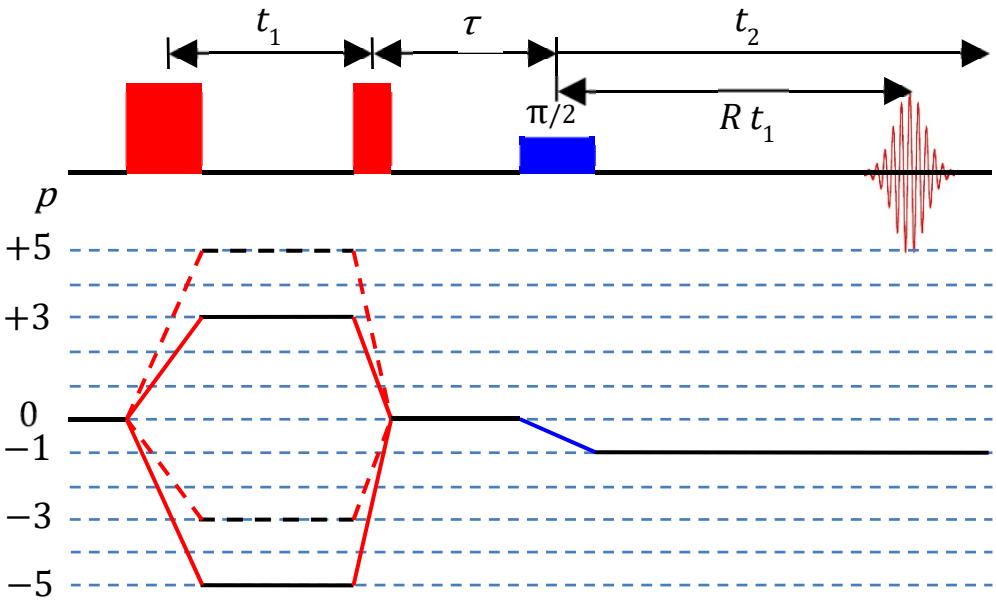

Fig. 5.1. Pulse sequence and coherence transfer pathways for *z*-filter 3QMAS and 5QMAS in the level diagram for spin-5/2 nuclei. The antiecho pathways are dashed. The duration τ lasts for a few MAS rotation periods.

Quantum mechanics allows transitions only for $\Delta p = 1$. Multiple-quantum transitions are forbidden. In other words, a pulse produces all multiple-quantum conversions with a lower probability than single-quantum conversions, and the probability decreases significantly with the number of the order. Furthermore, a special cycling of the pulse phase is necessary, in order to select the pathway of coherences by the pulse program.

The rotation of the spin density operator of coherence, σ^p, by the angle φ around the z-direction is described by

$$\sigma^p \xrightarrow{\varphi\, F_z} \sigma^p \exp(-\mathrm{i}p\varphi). \tag{5.03}$$

An RF pulse P with phase φ starts at the time t^-, ends at the time t^+ and transfers coherences from the order p^- to the order p^+. The influence of the pulse on the spin density operator is

$$P(\varphi)\, \sigma^{p^-}(t^-)\, P(\varphi)^{-1} = \sigma^{p^+}(t^+) \exp\{-\mathrm{i}\varphi(p^+ - p^-)\}. \tag{5.04}$$

Now, we consider the quintuple-quantum experiment in Fig. 5.1 and use 0° for the phases of the first and third pulses and for the receiver phase. But the phase of the second pulse is incremented in steps of 2π/5 (360/5)° starting from 0°. After five steps, the coherences at $p = +5$ and $p = -5$ are five times accumulated while almost all other coherences are averaged to zero, except for the coherence at $p = 0$, which is five times accumulated. In order to quench the coherences at $p = 0$, we increment ten times by (360/10)° and use alternating receiver phases of 0° and 180°. The signal for $p = 0$ is quenched after two scans with alternating receiver phases. After 10 scans we are left with the coherences at $p = \pm 5$ only. The phase cycling for all spins was described by Goldbourt and Madhu [3] in their Table 5b.

Phase cycling has to be further prolonged by a cyclically ordered phase sequence (CYCLOPS) for the 1D quadrature detection in t_2 and by the States method [7], which uses signal acquisition from two complementary experiments to provide the real and imaginary parts in t_1, thereby allowing the 2D-Fourier-transform in the F_1-direction.

The optimum durations of the first and second strong pulses have to be calibrated, in order to obtain the maximum generation of the desired coherences and the maximum possible transfer of coherences between the desired p-levels, respectively. They depend as usual on the RF power, but also on the p-levels, the MAS frequency, and the quadrupole parameters. The latter means that an approximate knowledge about the quadrupole parameters of the system under study is a precondition. The optimization on the spectrometer requires a long measuring time, especially for weak signals. Numerical simulations are more convenient, and the use of the SIMPSON package is recommended for this purpose [8]. If simulations or other additional information are not available, the experiment should be started with non-selective flip angles of about 180° and 50° for the first and second pulse, respectively. The same holds for the split-t_1 method, which is discussed in Section 5.3.

5.2 Shearing and Scaling

The assignment of the resonance shifts along the F_2 and F_1 dimensions of the 2D spectrum cannot be done in a straight way, if the spectrum was acquired by means of the z-filter pulse sequence or other sequences for which t_1 equals the spacing between the two strong pulses. For a simpler analysis of the 2D spectrum, we introduce in addition to the axis A with the slope $R(I,p)$ the isotropic chemical shift axis CS. This axis describes the variable isotropic chemical shift in the case of the zero quadrupole shift, has the slope 1, and crosses the coordinates $(0, 0)$, see Fig. 5.2. The third axis QIS has the slope $-10/17$ (see below), and describes variable quadrupole shifts at those values of the chemical shift, at which the axis QIS crosses the axis CS. Then we perform a shearing transform of the 2D spectrum, which results in a parallel orientation of the axis A and the new axis $F_1 = F_{\mathrm{ISO}}$. Now the orthogonal projection of the 2D spectrum onto the new axis $F_1 = F_{\mathrm{ISO}}$ does not include anisotropic contributions; see Fig. 5.2. The shearing can usually be performed by an additional program in the processing software of the spectrometer.

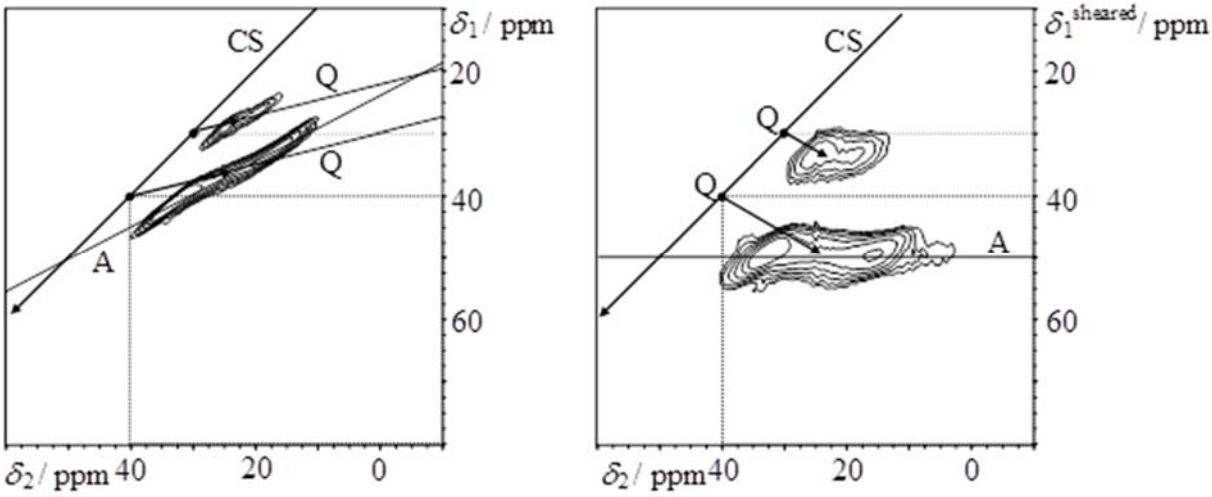

Fig. 5.2. 2D ^{17}O 3QMAS NMR spectra of the zeolite Na-ZSM-5 after the 2D Fourier transform (left) and after the following shearing transform (right). The two signals were assigned to SiOSi and SiOAl fragments with concentrations of 80% and 20%, $\boldsymbol{\delta}_{\mathrm{iso\,CS}}$ = 40 and 30 ppm, C_Q = 5.3 and 3.5 MHz, $\boldsymbol{\eta}$ = 0.12 and 0.29, respectively [9].

The scaling of the axes [10] starts from the isotropic part of Eq. 5.01. We use a zero-offset and obtain

$$\nu_{\mathrm{iso}} = \sigma_{\mathrm{iso}}\nu_{\mathrm{L}}p + \nu_{\mathrm{iso\,Q}} = \sigma_{\mathrm{iso}}\nu_{\mathrm{L}}p + \frac{10^6\nu_{\mathrm{Q}}^2 p}{30\,\nu_{\mathrm{L}}}\left[I(I+1) - \frac{3}{4}p^2\right]\left(1 + \frac{\eta^2}{3}\right). \tag{5.05}$$

Multiplication by $10^6/(-p\nu_{\mathrm{L}})$ transforms the frequency scale into the ppm scale. The denominator $-p\nu_{\mathrm{L}}$ describes the apparent Larmor frequency and includes the real Larmor frequency for $p = -1$. For the F_1 axis (before shearing) we have

$$\delta_1 = \delta_{\mathrm{iso\,CS}} + \delta_{\mathrm{iso\,Q}} = \delta_{\mathrm{iso\,CS}} - \frac{10^6\nu_{\mathrm{Q}}^2}{30\,\nu_{\mathrm{L}}}\left[I(I+1) - \frac{3}{4}p^2\right]\left(1 + \frac{\eta^2}{3}\right). \tag{5.06}$$

The F_2 axis is independent of p:

$$\delta_2 = \delta_{\mathrm{iso\,CS}} + \delta_{\mathrm{iso\,Q}} = \delta_{\mathrm{iso\,CS}} - \frac{10^6\nu_{\mathrm{Q}}^2}{30\,\nu_{\mathrm{L}}}\left[I(I+1) - \frac{3}{4}\right]\left(1 + \frac{\eta^2}{3}\right). \tag{5.07}$$

Eq. (5.06) describes the shift δ_2 of the center of gravity of the anisotropic ridge, which is not influenced by the shearing transformation. But the δ_1 changes after shearing and becomes [11]

$$\begin{aligned}\delta_1^{\mathrm{sheared}} &= \delta_{\mathrm{iso\,CS}} - \frac{-10}{17}\frac{10^6\,\nu_{\mathrm{Q}}^2}{30\,\nu_{\mathrm{L}}}\left[I(I+1) - \frac{3}{4}\right]\left(1 + \frac{\eta^2}{3}\right) \\ &= \delta_{\mathrm{iso\,CS}} + \frac{10^6\nu_{\mathrm{Q}}^2}{51\,\nu_{\mathrm{L}}}\left[I(I+1) - \frac{3}{4}\right]\left(1 + \frac{\eta^2}{3}\right).\end{aligned} \tag{5.08}$$

It can be seen that after shearing, the quadrupole shift is always positive and independent of p. The factor $-10/17$, which appears in Eq. (5.08), describes the slope of the axis QIS of variable quadrupole shifts. The shift difference between the crossing point (of QIS and CS axes) and the center of gravity of a signal gives the corresponding quadrupole shift $\delta_{\mathrm{iso\,Q}}^{\mathrm{sheared}}$.

One-dimensional anisotropic slices A can be obtained from the 2D spectrum and fit by a line-shape simulation. This gives values for ν_{Q} and η independently, whereas $\delta_{\mathrm{iso\,Q}}^{\mathrm{sheared}}$ is a function of $\nu_{\mathrm{Q}}^2\,(1 + \eta^2/3)$. The quadrupole parameter obtained from the 2D spectrum can be used finally for a simulation of the single-quantum MAS NMR spectrum. This procedure yields correct information about the relative concentrations of the various species giving rise to the corresponding signals.

5.3 Split-t_1 and Full-Echo Observation

The split-t_1 method is more often used than the *z*-filter method, since it avoids the necessity of an additional shearing of the 2D spectra. The basic idea is the splitting of the evolution time t_1 into multiple-quantum and single-quantum evolution periods in such a ratio that the fourth-order anisotropic term is refocused at the end of the t_1 period [5]. The pulse sequence consists of two hard pulses and two soft π/2-pulses in a symmetric coherence pathway for the observation of the FID (Fig. 5.3), or of two hard pulses and one soft π-pulse in an echo or antiecho pathway for the observation of a full echo (Fig. 5.4).

Fig. 5. 3 shows symmetric pathways with *z*-filter $0 \rightarrow \pm p \rightarrow \pm 1 \rightarrow 0 \rightarrow -1$ for $p = 2I$ coherences and $0 \rightarrow \pm p \rightarrow \mp 1 \rightarrow 0 \rightarrow -1$ for $p < 2I$ coherences. The latter experiment yields a lower signal-to-noise ratio, since it involves a higher multiple-quantum transition. As for all multiple-quantum experiments, the ν_{RF} of the first two pulses should be as high as possible, whereas the ν_{RF} of the π/2- or π-pulses should be so small that it only slightly exceeds the spectrum width of the central transition.

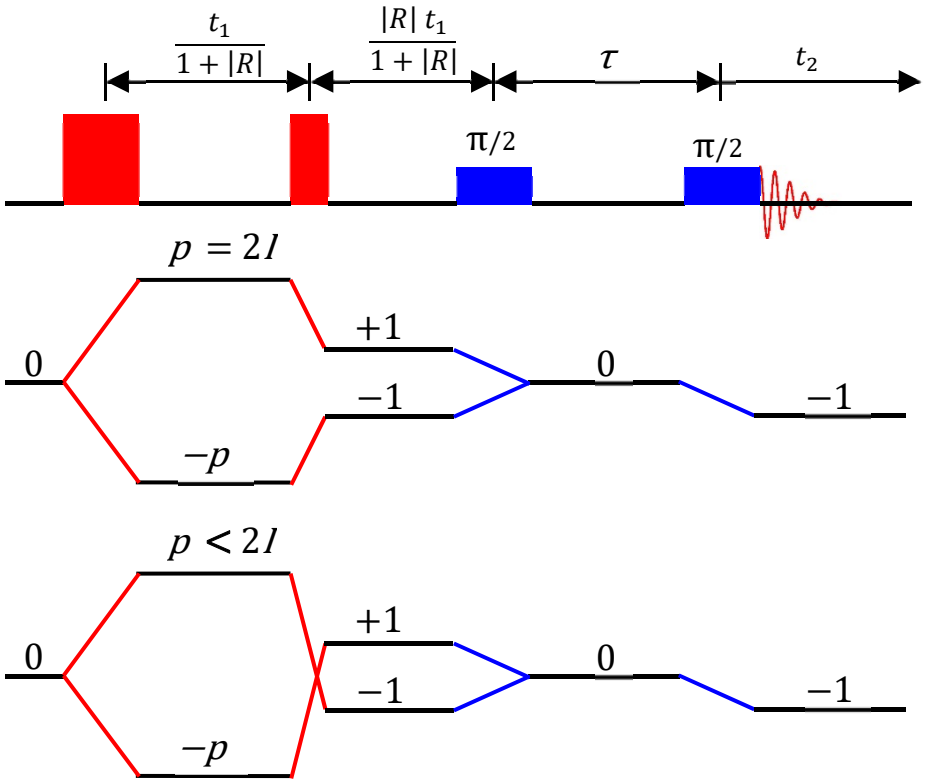

Fig. 5.3. Split-t_1 pulse sequence with time scale and symmetric coherence transfer pathways for the observation of the FID. The upper and lower pathways hold for multiple quantum coherences $p = 2I$ and $p < 2I$, respectively. The delay τ lasts for a few MAS rotation periods. The factor $R(I,p)$ is given in Eq. (5.02).

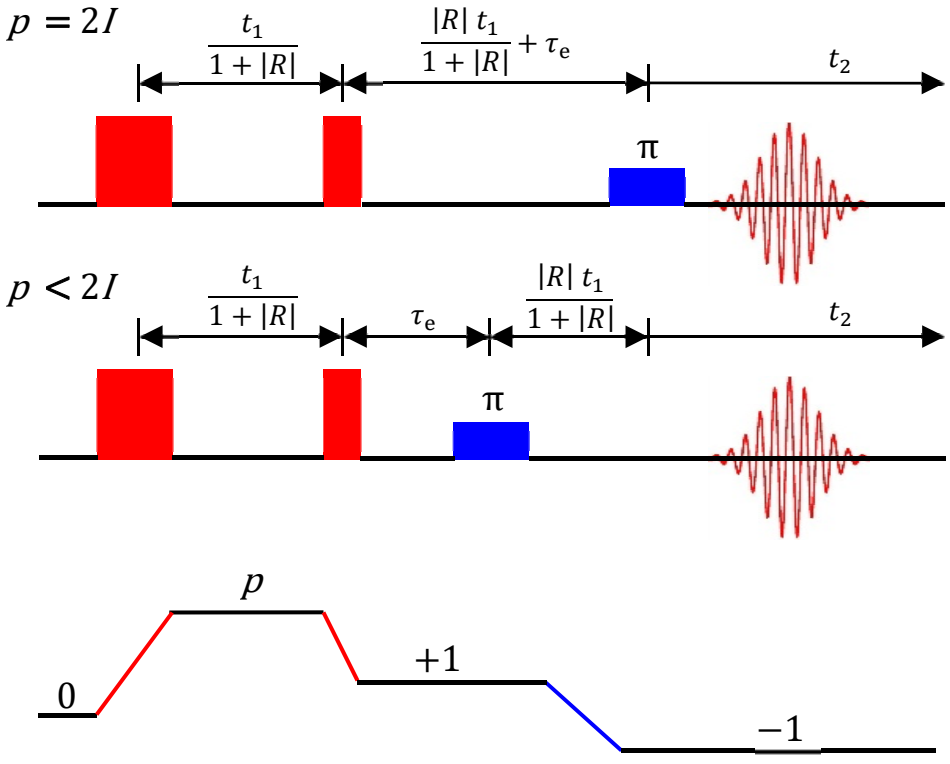

Fig. 5.4. Split-t_1 pulse sequence with time scales and the coherence transfer pathway for the observation of the full-shifted echo. The upper and lower time scales hold for multiple quantum coherences $p = 2I$ and $p < 2I$, respectively. The echo maximum appears at the time of the echo delay, $t_2 = \tau_e$. The factor $R(I,p)$ is given in Eq. (5.02).

Fig. 5.4 shows the split-t_1 pulse sequence for the observation of the full-shifted echo, which has been recommended [12-14] as the most efficient rectangular pulse sequence for MQMAS NMR, when the loss of magnetization due to $T_2^{\mathrm{MAS\ echo}}$ effects is not significant. Strong homonuclear dipolar interaction reduces the transverse relaxation time $T_2^{\mathrm{MAS\ echo}}$ and decreases the amplitude of the echo in Fig. 5.4 by the factor $\exp(-\frac{2\tau_e}{T_2^{\mathrm{MAS\ echo}}})$.

In case of spin-5/2 nuclei we have in Figs. 5.3 and 5.4 for $p = 5$ the t_1-splitting-factors of 12/37 and 25/37 and for $p = 3$ the factors 12/31 and 19/31. In case of the spin-3/2 nuclei we have only $p = 3$, and the factors are 9/16 and 7/16. The pathway in Fig. 5.4 shows the way for the antiecho in the cases $I = 5/2;\ p = 5$ and $I = 3/2;\ p = 3$, and it is the echo pathway for $I = 5/2;\ p = 3$. For the phase cycling of the shifted echo split-t_1 pulse sequence we refer to Goldbourt and Madhu [3] and their Tables 5c and 5d.

5.4 Enhancement of Sensitivity by RIACT, FAM, DFS, SPAM and CPMG

An alternative approach to the generation of triple-quantum transitions by strong pulses is the adiabatic transfer by the interchange between the eigenstates 3Q and 1Q undergoing MAS, the so-called rotation-induced adiabatic coherence transfer (RIACT), which was introduced by Wu *et al.* [15]. RIACT is explained in some recent reviews [2, 3, 16, 17], and the Web of Science shows 13 hits for RIACT studies in the years 1996-2009, the last one by Rovniak and Kennedy [18]. FASTER (fast spinning transfer enhancement at rotary resonance), a similar procedure using rotational resonance but with fewer applications, also works in the regime of weak and long RF pulses and was introduced and improved by Voosegart *et al.* [19, 20] .

One intention for the introduction of rotation-induced adiabatic coherence transfers for MQMAS was the enhancement of excitation. Excitation can also be enhanced by the application of a double-frequency sweep (DFS) [21] (see Section 2.9), or by fast RF amplitude modulation (FAM), which was introduced by Goldbourt *et al.* [3, 22]. The former uses an easily adjustable frequency modulation and the latter uses amplitude modulation, which can be performed on spectrometers for which frequency modulation of the short RF pulse is not feasible. There is no difference between DFS and FAM from a physical point of view, since frequency and phase modulations of the RF can give the same result. DFS and FAM are seldom used for the first, relatively short, excitation pulse of the MQMAS pulse sequence. But the use of DFS for the second, relatively longer, conversion pulse is now part of the standard MQMAS procedure. Colaux *et al.* [23] alternatively introduced the so-called FAM-N pulse for triple- to single-quantum coherence conversion. Experimental comparisons [12] have shown that the application of DFS or FAM improves the conversion by a factor of about two with respect to a rectangular conversion pulse.

SPAM (soft pulse-added mixing) was introduced by Gan and Kwak [24] as a modification of the *z*-filter and split-t_1 methods, in order to use the capacities of the 0Q and $\pm$1Q coherence levels simultaneously. Hard and soft pulses directly follow each other, in order to form a composite SPAM conversion sequence which is specially recommended [25] for the $\pm 3 \rightarrow \mp 1$ coherence transfer; see Fig. 5.3. The general advantage or SPAM pulses is that they do not require the iterative optimization of two hard pulses [25]. Amoureux *et al.* [26] found an intensity enhancement up to 3 times the intensity. Critical evaluations of different SPAM applications were given by Ball and Wimperis [25].

The application of CPMG (see Sect. 3.9) was also used, in order to increase the signal-to-noise ratio of MQMAS spectra, and some examples of this application can be found in the literature [27-29].

5.5 Sensitivity and Resolution

Section 5.4 describes some techniques that can increase the signal-to-noise ratio of the spectra by a factor in the range 2−3. This is important, since MQMAS NMR spectroscopy is a relatively insensitive technique. The determination of the signal-to-noise ratios of a the ^{27}Al NMR spectra of $ALPO_4$-14 in 2.5-mm-rotors with a recycle delay of 0.5 s, spinning frequencies of 4 kHz (inner) for DOR and 30 kHz for MAS, a Larmor frequency of 195 MHz and a measuring time of 10 h gave for MAS, DOR, 3QMAS with DFS and 5QMAS with DFS the values of 4222, 2791, 149 and 75, respectively [12]. The low efficiency of the multiple-quantum transitions and the necessity of the acquisition of a 2D spectrum drastically lower the signal-to-noise ratios. Practically speaking, a MQMAS spectrum usually needs an overnight run. We can also conclude that the 5QMAS intensity is reduced by a factor of 2 with respect to 3QMAS. A more important disadvantage for 5Q compared to 3QMAS is the smaller spectral window, which has for rotation-synchronized experiments (in order to avoid spinning sidebands) at ν_{MAS} =30 kHz and ν_{L} =195 MHz for 3QMAS and 5QMAS the widths of about 110 ppm and 22 ppm, respectively.

We consider two broadening mechanism of the signals for the discussion of the spectral resolution. "Chemical" broadening of the signals is caused mainly by a distribution of the isotropic chemical shift. It occurs in solid non-crystalline materials and also in crystalline materials with ill-defined short range order like zeolites (except pure siliceous material), which contain silicon, aluminum and ions on extra-framework positions. The distribution of isotropic quadrupole shifts (distribution of quadrupole parameters) can also be caused by the distribution of bond angles in the solid. But this causes a smaller effect than the chemical shift distribution [30]. The "chemical" broadening can be detected by means of other resonances, e. g. by ^{29}Si MAS NMR for zeolites. Freude *et al.* [30] estimated the "chemical" broadening of ^{17}O 3QMAS and 5QMAS NMR spectra of zeolites LSX by means of the broadening of the measured ^{29}Si MAS NMR spectra of the samples. The dominance of chemical broadening can be claimed if the broadening of a signal, expressed in ppm, does not change upon changing the external magnetic field. It should be noted that "chemical" broadening cannot be removed by any NMR technique without removing the chemical shift.

Signal broadening by the anisotropy of the second-order quadrupole interaction is reciprocal to the squared external magnetic field on the ppm scale. It does not occur, if DOR or MQMAS is properly applied. On the frequency scale, dipolar broadening is independent of the external magnetic field. It should be removed upon very fast magic-angle spinning. But a strong homonuclear dipolar interaction could not be removed by MAS at 30 kHz; see the end of Section 3.9. This means that we have to consider a residual homonuclear dipolar broadening of the MQMAS signals, as discussed in a study by Amoureux and Trébosc [31]. A similar effect takes place when strong dipolar coupling exists between adjacent hetero nuclei. This broadening is field-independent in Hz, whereas the residual line width is commonly expressed in ppm. These facts explain the two findings that for the well-crystallized material $ALPO_4$-14 the resolution of the ^{27}Al MQ MAS spectra is increased by a factor of about 2 (theoretically 17.6/9.4) if the external magnetic field is increased from 9.4 T to 17.6 T, while the resolution is increased by a factor of about 2 (theoretically 5/3) if 5QMAS is used instead of 3QMAS [12]. However, due to the explanations in the previous paragraph, an increase of resolution from 3QMAS to 5QMAS could not be found for the ^{17}O spectra of zeolite LSX [30], for which a disturbed short-range order causes a "chemical" broadening.

5.6 Combinations of MQMAS with 1QCP, MQCP, HETCOR, TEDOR and REDOR

MQMAS techniques have been combined with other solid-state NMR procedures in order to get highly resolved spectra with information about nuclear correlations like hetero- and homonuclear through-space dipolar couplings and so-called "scalar" through-bond heteronuclear couplings or J couplings between the observed nuclei and their spin-1/2 or quadrupolar neighbors [32]. Single- and multiple-quantum cross-polarization excitations have the acronyms 1QCP and MQCP, respectively [33]. The dipolar heteronuclear correlation experiment (MQMAS-D-HETCOR) is performed by spin-locking the MQMAS echo after the second strong pulse, followed by CP transfer and starting the signal acquisition in the spin-1/2 channel [34, 35]. Spin-locking of the echo and cross-polarization can be substituted by using J-couplings (MQMAS-J-HETCOR), although they are weaker than dipolar couplings in solids [36]. The correct spinlock of quadrupolar nuclei to high-γ spin-1/2 nuclei requires very weak RF fields during the mixing time and leads to poor sensitivity [37]. This can be avoided using the TEDOR-scheme (transferred echo double-resonance) instead of CP in MQMAS experiments [37-39]. The technique is now established as dipolar heteronuclear multiple-quantum coherence (D-HMQC) [40]. *Wang et al.* [41] showed that the manipulation of the satellite transitions can accelerate and enhance coherence transfer to spin-1/2 nuclei and called the technique population transfer heteronuclear multiple-quantum correlation (PT-HMQC). The technique is also efficient to enhance the sensitivity of *J*-mediated heteronuclear correlation experiments between two half-integer quadrupolar nuclei [42]. Rotational echo double resonance (REDOR) avoids CP as well, and has been used in combination with MQMAS to measure distances between ^{19}F and ^{27}Al pairs [32]. The combinations published before 2012 are described in detail in the review by Fernandez and Pruski [17].

5.7 References

[1] L. Frydman, J.S. Harwood, Isotropic Spectra of Half-integer Quadrupolar Spins from Bidimensional Magic-angle Spinning NMR, J. Am. Chem. Soc. 117 (1995) 5367-5368.

[2] J.-P. Amoureux, M. Pruski, MQMAS NMR: Experimental Strategies, in: R.E. Wasylishen, S.E. Ashbrook, S. Wimperis (Eds.) NMR of Quadrupolar Nuclei in Solid Materials, Wiley, Chichester, 2012, pp. 143-162.

[3] A. Goldbourt, P.K. Madhu, Multiple-quantum Magic-angle Spinning: High-resolution Solid-state NMR of Half-integer Spin Quadrupolar Nuclei, Annu. Rep. Nucl. Magn. Reson. Spectrosc. 54 (2005) 81-153.

[4] J.P. Amoureux, C. Fernandez, S. Steuernagel, Z-Filtering in MQMAS NMR, J. Magn. Reson. A 123 (1996) 116-118.

[5] S.P. Brown, S.J. Heyes, S. Wimperis, Two-dimensional MAS Multiple-quantum NMR of Quadrupolar Nuclei, Removal of Inhomogeneous Second-order Broadening, J. Magn. Reson. A 119 (1996) 280-284.

[6] C. Fernandez, J.P. Amoureux, Triple-quantum MAS-NMR of Quadrupolar Nuclei, Solid State Nucl. Magn. Reson. 5 (1996) 315-321.

[7] D.J. States, R.A. Haberkorn, D.J. Ruben, A Two-Dimensional Nuclear Overhauser Experiment with Pure Absorption Phase in Four Quadrants, J. Magn. Reson. 48 (1982) 286-292.

[8] M. Bak, J.T. Rasmussen, N.C. Nielsen, SIMPSON: A General Simulation Program for Solid-state NMR Spectroscopy, J. Magn. Reson. 147 (2000) 296-330.

[9] U. Pingel, ^{17}O NMR -Spektroskopie von Porösen Materialien, PhD thesis, Universität Leipzig, Leipzig, 2000.

[10] D. Freude, Quadrupole Nuclei in Solid-state NMR, in: R.A. Meyers (Ed.) Encyclopedia of Analytical Chemistry, John Wiley & Sons, Chichester, 2000, pp. 12188-12224.

[11] J.P. Amoureux, C. Fernandez, Triple, Quintuple and Higher Orders Multiple Quantum MAS NMR of Quadrupolar Nuclei, Solid State Nucl. Magn. Reson. 10 (1998) 211-224.

[12] J. Kanellopoulos, D. Freude, A. Kentgens, A Practical Comparison of MQMAS Techniques, Solid State Nucl. Magn. Reson. 32 (2007) 99-108.

[13] M. Pruski, J.W. Wiench, J.P. Amoureux, On the Conversion of Triple- to Single-quantum Coherences in MQMAS NMR, J. Magn. Reson. 147 (2000) 286-295.

[14] S.P. Brown, S. Wimperis, Two-Dimensional Multiple-Quantum MAS NMR of Quadrupolar Nuclei: A Comparison of Methods, J. Magn. Reson. 128 (1997) 42-61.

[15] G. Wu, D. Rovnyak, R.G. Griffin, Quantitative Multiple-quantum Magic-angle Spinning NMR Spectroscopy of Quadrupolar Nuclei in Solids, J. Am. Chem. Soc. 118 (1996) 9326-9332.

[16] J.-P. Amoureux, M. Pruski, MQMAS NMR: Experimental Strategies and Applications, in: R.K. Harris, R.E. Wasylishen (Eds.) Encyclopedia of Magnetic Resonance, Wiley, Chichester, 2009, pp. 143-162.

[17] C. Fernandez, M. Pruski, Probing Quadrupolar Nuclei by Solid-State NMR Spectroscopy: Recent Advances, Top. Curr. Chem. 306 (2012) 119-188.

[18] D. Rovnyak, P.E. Kennedy, Application of Shaped Adiabatic Pulses to MQMAS NMR Spectroscopy of Spin 3/2 Nuclei, J. Magn. Reson. 196 (2009) 191-199.

[19] T. Vosegaard, P. Florian, D. Massiot, P.J. Grandinetti, Multiple-quantum Magic-angle Spinning Using Rotary Resonance Excitation, J. Chem. Phys. 114 (2001) 4618-4624.

[20] T. Vosegaard, C. Kehlet, N. Khaneja, S.J. Glaser, N.C. Nielsen, Improved Excitation Schemes for Multiple-quantum Magic-angle Spinning for Quadrupolar Nuclei Designed Using Optimal Control Theory, J. Am. Chem. Soc. 127 (2005) 13768-13769.

[21] A.P.M. Kentgens, R. Verhagen, Advantages of Double Frequency Sweeps in Static, MAS and MQMAS NMR of Spin *I* = 3/2 Nuclei, Chem. Phys. Lett. 300 (1999) 435-443.

[22] A. Goldbourt, P.K. Madhu, L. Frydman, S. Vega, Fast rf amplitude modulation in MQMAS NMR spectroscopy, Abstracts of the 41st Rocky Mountain Conference (1999) 97-98.

[23] H. Colaux, D.M. Dawson, S.E. Ashbrook, Efficient Amplitude-Modulated Pulses for Triple- to Single-Quantum Coherence Conversion in MQMAS NMR, J. Phys. Chem. A 118 (2014) 6018-6025.

[24] Z.H. Gan, H.T. Kwak, Enhancing MQMAS Sensitivity Using Signals from Multiple Coherence Transfer Pathways, J. Magn. Reson. 168 (2004) 346-351.

[25] T.J. Ball, S. Wimperis, Use of SPAM and FAM Pulses in High-resolution MAS NMR Spectroscopy of Quadrupolar Nuclei, J. Magn. Reson. 187 (2007) 343-351.

[26] J.P. Amoureux, L. Delevoye, S. Steuernagel, Z. Gan, S. Ganapathy, L. Montagne, Increasing the Sensitivity of 2D High-resolution NMR Methods Applied to Quadrupolar Nuclei, J. Magn. Reson. 172 (2005) 268-278.

[27] F.H. Larsen, I. Farnan, Site Populations and Short Range Order in Aluminosilicates Investigated by ^{27}Al solid-state NMR, J. Phys. Chem. B 108 (2004) 9764-9771.

[28] R. Lefort, J.W. Wiench, M. Pruski, J.P. Amoureux, Optimization of Data Acquisition and Processing in Carr-Purcell-Meiboom-Gill Multiple Quantum Magic Angle Spinning NMR J. Chem. Phys. 116 (2002) 2493-2501.

[29] T. Vosegaard, F.H. Larsen, H.J. Jakobsen, P.D. Ellis, N.C. Nielsen, Sensitivity-enhanced Multiple-quantum MAS NMR of Half-integer Quadrupolar Nuclei, J. Am. Chem. Soc. 119 (1997) 9055-9056.

[30] D. Freude, T. Loeser, D. Michel, U. Pingel, D. Prochnow, ^{17}O NMR Studies of Low Silicate Zeolites, Solid State Nucl. Magn. Reson. 20 (2001) 46-60.

[31] J.P. Amoureux, J. Trebosc, Homogeneous Broadenings in 2D Solid-state NMR of Half-integer Quadrupolar Nuclei, J. Magn. Reson. 179 (2006) 311-316.

[32] C. Fernandez, D.P. Lang, J.P. Amoureux, M. Pruski, Measurement of Heteronuclear Dipolar Interactions between Quadrupolar and Spin-1/2 Nuclei in Solids by Multiple-quantum REDOR NMR, J. Am. Chem. Soc. 120 (1998) 2672-2673.

[33] S.E. Ashbrook, S. Wimperis, Multiple-quantum Cross-polarization and Two-dimensional MQMAS NMR of Quadrupolar Nuclei, J. Magn. Reson. 147 (2000) 238-249.

[34] S.H. Wang, S.M. DePaul, L.M. Bull, High-resolution Heteronuclear Correlation between Quadrupolar and Spin-1/2 Nuclei Using Multiple-quantum Magic-angle Spinning, J. Magn. Reson. 125 (1997) 364-368.

[35] C. Fernandez, C. Morais, J. Rocha, M. Pruski, High-resolution Heteronuclear Correlation Spectra between P-31 and Al-27 in Microporous Aluminophosphates, Solid State Nucl. Magn. Reson. 21 (2002) 61-70.

[36] D. Massiot, F. Fayon, B. Alonso, J. Trebosc, J.P. Amoureux, Chemical Bonding Differences Evidenced from J-coupling in Solid State NMR Experiments Involving Quadrupolar Nuclei, J. Magn. Reson. 164 (2003) 160-164.

[37] J.P. Amoureux, J. Trebosc, G. Tricot, Measurement of Through-space Connectivities between Spin-1/2 and Quadrupolar Nuclei in Solid-state NMR: The TEDOR-MQMAS Method, Magn. Reson. Chem. 45 (2007) S187-S191.

[38] Z. Gan, ^{13}C/^{14}N Heteronuclear Multiple-quantum Correlation with Rotary Resonance and REDOR Dipolar Recoupling, J. Magn. Reson. 184 (2007) 39-43.

[39] J. Trebosc, B. Hu, J.P. Amoureux, Z. Gan, Through-space R3-HETCOR Experiments between Spin-1/2 and Half-integer Quadrupolar Nuclei in Solid-state NMR, J. Magn. Reson. 186 (2007) 220-227.

[40] G. Tricot, J. Trébosc, F. Pourpoint, R. Gauvin, L. Delevoye, The D-HMQC MAS-NMR Technique: An Efficient Tool for the Editing of Through-Space Correlation Spectra Between Quadrupolar and Spin-1/2 (^{31}P, ^{29}Si, ^{1}H, ^{13}C) Nuclei, in: A.W. Graham (Ed.) Annu. Rep. NMR Spectr., Academic Press, 2014, pp. 145-184.

[41] Q. Wang, J. Trebosc, Y.X. Li, J. Xu, B.W. Hu, N.D. Feng, Q. Chen, O. Lafon, J.P. Amoureux, F. Deng, Signal Enhancement of J-HMQC Experiments in Solid-state NMR Involving Half-integer Quadrupolar Nuclei, Chem. Comm. 49 (2013) 6653-6655.

[42] Q. Wang, Y.X. Li, J. Trebosc, O. Lafon, J. Xu, B.W. Hu, N.D. Feng, Q. Chen, J.P. Amoureux, F. Deng, Population Transfer HMQC for Half-integer Quadrupolar Nuclei, J. Chem Phys 142 (2015).